

Reply to Reviewer #3

Dear Prof. Montgomery:

We thank you very much for your time and efforts in reviewing our manuscript. All of your comments and suggestions have been carefully taken into consideration. Please find our point-by-point responses below.

Summary:

The authors conduct two numerical experiments using the WRF model and attempt to explain why one experiment undergoes secondary eyewall formation (SEF), while the other does not.

Evaluation:

The authors conduct two numerical simulations, one with higher horizontal resolution than the other. Based on these two solutions, the authors argue that “the structure of the eyewall can play an important role in secondary eyewall formation”. The authors find that in the higher horizontal resolution simulation “the eyewall is more upright with stronger updrafts, accompanied by a wide eyewall anvil at a higher altitude.” However, it is unclear to this reviewer why such eyewall features are central to SEF.

The authors claim to offer an interpretation for why the higher resolution experiment undergoes SEF. The interpretation seems to hinge on a mixed cloud-physics and balance equation explanation highlighting the “cooling outside the inner eyewall ... induced by the sublimation, melting and evaporation of hydrometeors falling from the eyewall anvil.” The authors claim to have shown that: “The cooling ... *induces upper-level dry, cool inflow below the anvil, prompting the subsidence and moat formation between the inner eyewall and the spiral rainband*” (emphasis mine).

The authors hypothesize that the formation of a moat between the inner eyewall and spiral rainband is an essential precursor for the formation of SEF in their experiments. However, there is little, if any, consistent dynamical analysis offered to support this hypothesis. The only dynamical framework invoked to interpret their numerical

solutions is the Eliassen equation (their Eq. (2)) in radius-height coordinates, a formulation first developed by Smith et al. 2005. Unfortunately, the authors fail to explain how the coefficients of this partial differential equation are defined in their own solutions¹. Equally problematic is that no explanation of the Eliassen solution method is given for regions of negative static stability, negative absolute vorticity or negative symmetric stability. One or more of these possibilities generally occur in realistic simulations of a tropical cyclone (Wang et al. 2020, Wang et al. 2021). An important, but subtle, discovery found in Wang et al. 2021 was that the upper-level cool inflow below the anvil is incorrectly characterized as a balanced flow feature. In the Eliassen model, this localized upper-level inflow is an artifact of regularization, a procedure that is required to solve the Eliassen equation as an elliptic partial differential equation. In contrast, in the numerical simulations, the upper-level inflow is tied fundamentally to the agradient (unbalanced) force field in the upper tropospheric outflow region.

Thus, the balanced interpretation offered in this study for “the upper level dry, cool inflow below the anvil” is problematic. In view of this problem, the underlying explanation offered to explain SEF in the one experiment and not the other collapses.

Recommendation:

Do not accept. If the authors choose to revise their manuscript and resubmit to this journal, it should be required that the authors 1) cite these references given above, 2) discuss how the authors have addressed the issues raised in these references and 3) develop a physically consistent dynamical explanation for the occurrence of SEF in the one simulation and not the other.

Reply: Based on your suggestions, we have revised our manuscript by citing these important references you provided (**recommendation#1**), adding more discussions on

¹ Recent work has demonstrated important differences in the solutions of the Eliassen equation using a strictly balanced basic state vortex versus an unbalanced vortex that does not satisfy thermal wind balance (Montgomery and Persing 2020).

the issues raised in these references (i.e., the agradient (unbalanced) force and the connection between the cooling to the boundary layer processes and the mechanisms forcing the secondary eyewall formation, **recommendation#2&3**), adding figures and related discussions to the dynamical explanations of SEF (**recommendation#3**), and clarifying the definition of the coefficients and methodology for solving the SE equation (**Major comments**). Please refer to the detailed responses to your comments below.

(1) SE equation:

In this study, the SEE *is solved for the quadrant-mean field using the WRF output at 1-h intervals*. The quadrant-mean tangential wind and potential temperature are smoothed by 10 passes of a 1-2-1 smoother before solving the SEE, which can reduce the problematic issues in solving the SEE as done by Zhu and Zhu (2014). The heating forcing term is obtained directly from WRF outputs. The solver of the Multigrid Software For Elliptic Partial Differential Equations (Adams 1989) is used to solve the differential equation. The boundary conditions are set to $\Psi = 0$ at $r=0$ km, $z=0$ km, and $z=18$ km and $\frac{\partial \Psi}{\partial r} = 0$ at $r=110$ km.

For grid points *where the ellipticity condition is not satisfied*, we followed the method used by Heng et al. (2017). When the absolute vertical vorticity was negative, we replace the absolute negative vertical vorticity with a small positive value (0.01f). For other points with the discriminant not larger than zero, we reduced the vertical wind shear of the mean tangential wind by iterations until the ellipticity condition is satisfied.

As stated in Montgomery and Persing (2021), *the method we used to solve SEE is called the “pseudobalance” solution*. The mean vortex is not strictly in gradient wind and hydrostatic balance (see Figs. R3.1 and R3.2), but the “pseudobalance” solution is close to the model simulated secondary circulation (see Fig. R3.3), which is consistent with results from Heng et al. (2017) and from Fig. 5 shown in Montgomery and Persing (2021).

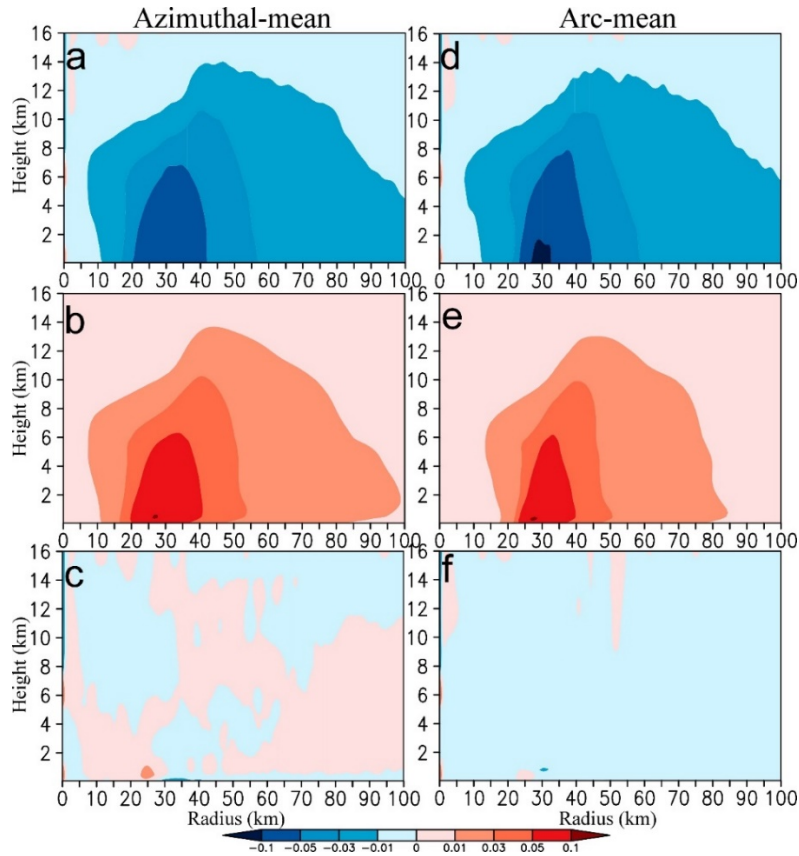


Figure R3.1 Radius-height cross-section of the (a-c) azimuthal- and (d-f) quadrant-mean (a, d) radial gradient force, (b, e) the sum of the centrifugal and Coriolis force, and (c, f) the agradient force at 30 h of the simulation.

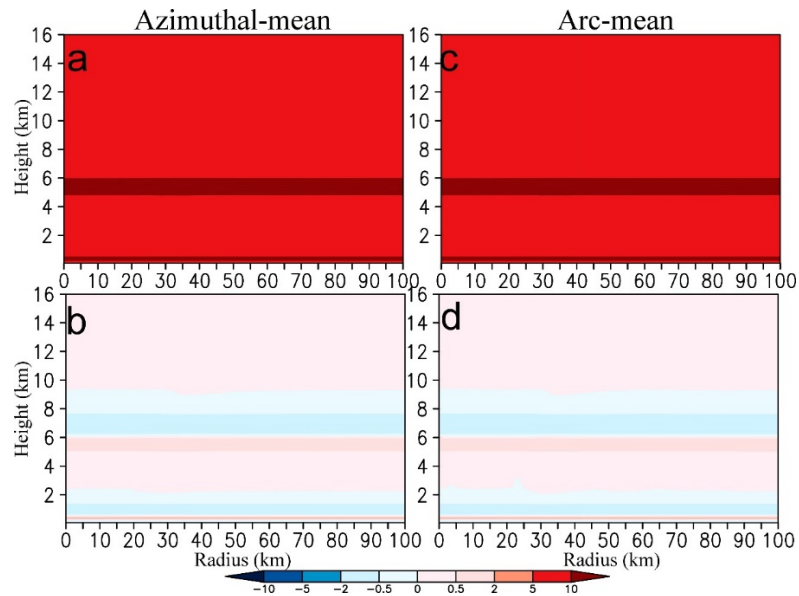


Figure R3.2 Radius-height cross-section of the (a, b) azimuthal- and (c, d) quadrant-mean (a, c) vertical gradient force, and (b, d) non-hydrostatic force at 30 h of the simulation.

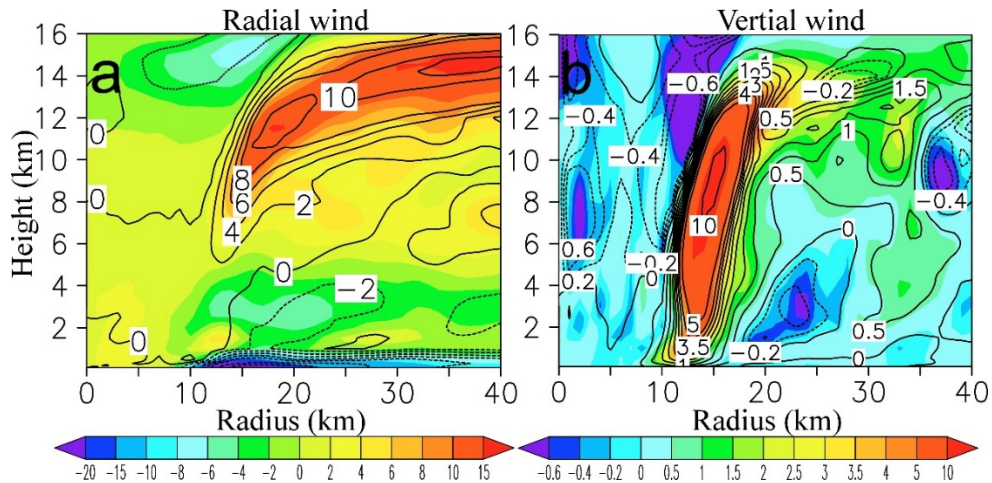


Figure R3.3 Radius-height cross-section of the quadrant-mean (a) radial and (b) vertical wind from the SEE-diagnosed (contours, m s^{-1}) and model output (shaded, m s^{-1}) results. The data is from the 5-min WRF output data at a 1-km resolution of Hurricane Wilma (2005).

(2) Unbalanced force associated with the upper-level inflow:

Previous studies have confirmed that the radial gradient force determines the inflows (Montgomery et al. 2020; Wang et al. 2020; Wang et al. 2021). Focusing on the upper-level inflows below the outflow layer, *we examine the gradient force in Fig. R3.4* in terms of the azimuthal and the quadrantal mean to understand the upper-level inflows. The gradient wind exists especially within the boundary layer, along the slantwise eyewall, and within the outflow layer. Inward gradient force persists and will accelerate the parcels inwards below the outflow layer and outside the eyewall, which is more significant in the quadrant-mean results, indicating that the upper-level inflow can be accelerated by the inward gradient force.

We highlighted the importance of the gradient force in the acceleration of the inflows in our revision, and we also believed that both the balanced and unbalanced forces determine the upper-level inflow. Based on your suggestion, we referred to those studies (Montgomery et al. 2020; Wang et al. 2020; Wang et al. 2021), and related discussions are added in the revision:

Previous studies indicated that the gradient force determines the inflows in TCs (Montgomery et al. 2020; Wang et al. 2020; Wang et al. 2021). We also examine the gradient force (not shown here) and confirm that the upper-level inflow is associated with the inward gradient force. The inward gradient force will accelerate the parcels

inwards below the outflow layer, suggesting that both the balanced and unbalanced processes are important to the evolution of the upper-level inflow.

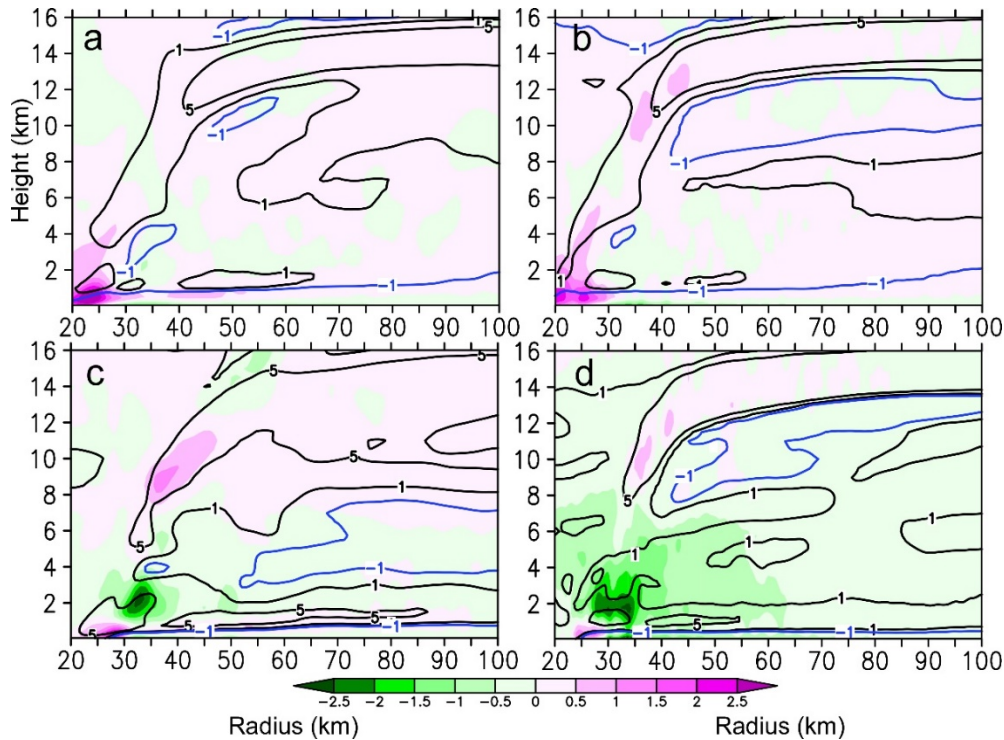


Figure. R3.4 Radius-height cross-sections of the (a, b) azimuthal-mean and (c, d) upshear-right quadrant-mean agradiant force (shaded, $10^{-2} \text{ m s}^{-1} \text{ s}^{-1}$) and the radial wind (outflows of 1 and 5 m s^{-1} in black lines and inflows of -1 m s^{-1} in blue lines) at 30 h for (a, c) NSEF and (b, d) CTL.

(3) Physically consistent dynamical explanation for SEF:

In this study, we found, in response to the diabatic warming in the eyewall with strong updrafts and large quantities of hydrometeors, an upper-level dry inflow occurs below the anvil. The drying effects caused by the inflow enhance diabatic cooling below the anvil, which causes negative buoyancy and prompts the subsidence. As feedback, the diabatic cooling further enhances the upper-level inflow. The moat forms with subsidence, which separates the inner eyewall from the outer convection. We also examine the agradiant force and confirm that the upper-level inflow is associated with inward agradiant forces. The inward agradiant force will accelerate the parcels inwards below the outflow layer, suggesting that both the balanced and unbalanced processes are important to the evolution of the upper-level inflow.

One additional aspect lacking in the current manuscript is a connection between the cooling to the boundary layer processes and the mechanisms forcing the secondary

eyewall formation. *In this revision, we added more discussions on the SEF related to the changes in the boundary layer forcing.* Figures R3.5 and R3.6 show that the moat subsidence (gray lines in Fig. R3.6b) descends into the boundary layer and its related divergent flow meets with the boundary inflows outside the moat. As a result, convergence occurs at radii from 80 km to 120 km where the SEF occurs in CTL (Figure R3.5b). On the other hand, the middle-level moist inflows associated with the outer rainbands travel radially inward and also contribute to the SEF by intensifying the wind field through the inward transport of large angular momentum. In contrast, there is divergence appearing in NSEF from 100-km to 170-km radii, and strong convergence is located under the broad single eyewall in NSEF.

Figure R3.7 examines the azimuthal-time cross-sections of the convergence at radii of 80-120 km below 1-km height. *The notable feature for the SEF is the enhanced convergence within the boundary layer along with the azimuthal extension of the moat subsidence. The enhanced convergence forces convection and increases the axisymmetric tangential wind via the axisymmetric dynamical process with the large filamentation time (Terwey and Montgomery 2008).*

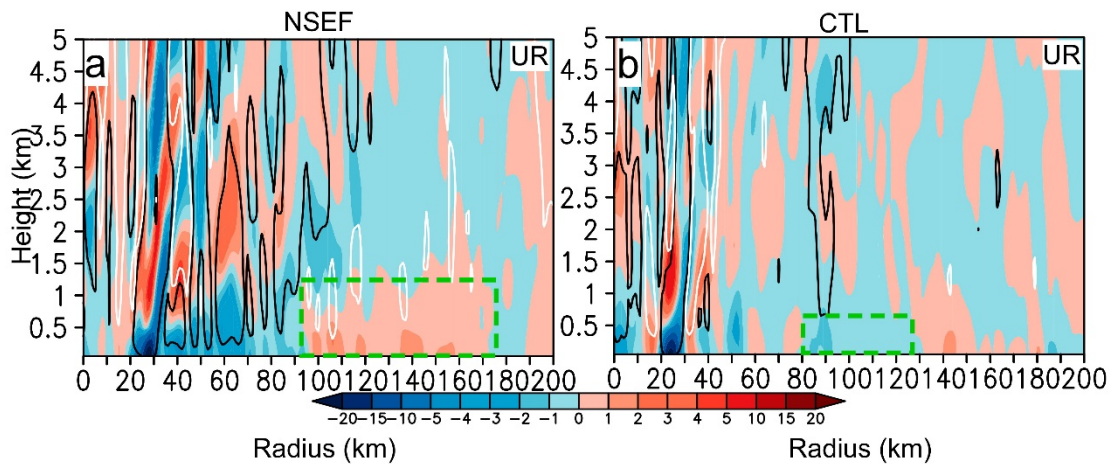


Figure. R3.5 Radius-height cross-sections of the quadrant-mean divergence (shaded, 10^{-4} s^{-1}) superimposed with the vertical wind (black lines of 0.1 m s^{-1} and white lines of -0.1 m s^{-1}) for the (a, b) upshear-right quadrant at 30 h for (a) NSEF and (b) CTL.

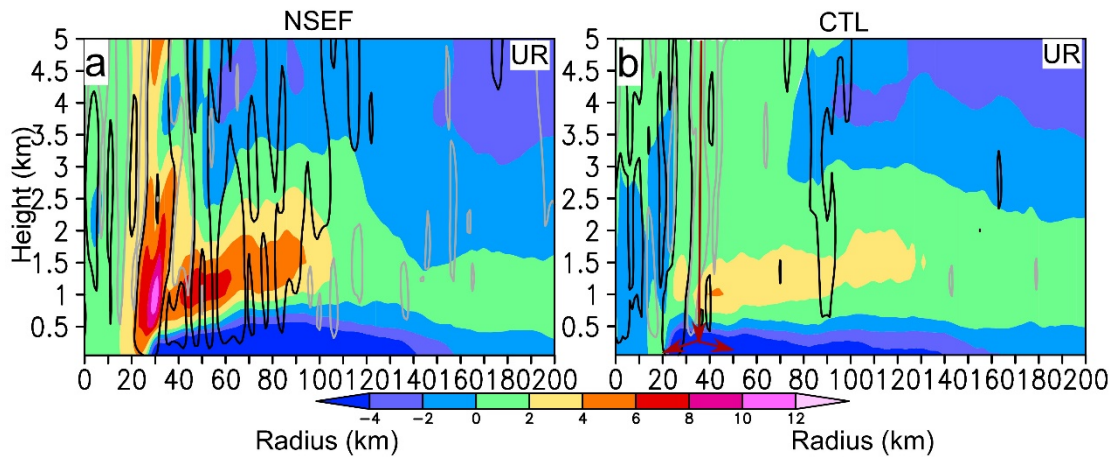


Figure. R3.6 Radius-height cross-sections of the quadrant-mean radial (shaded, m s^{-1}) superimposed with the vertical wind (black lines of 0.1 m s^{-1} and white lines of -0.1 m s^{-1}) for the (a, b) upshear-right quadrant at 30 h for (a) NSEF and (b) CTL. Red arrows indicate the subsidence and divergence.

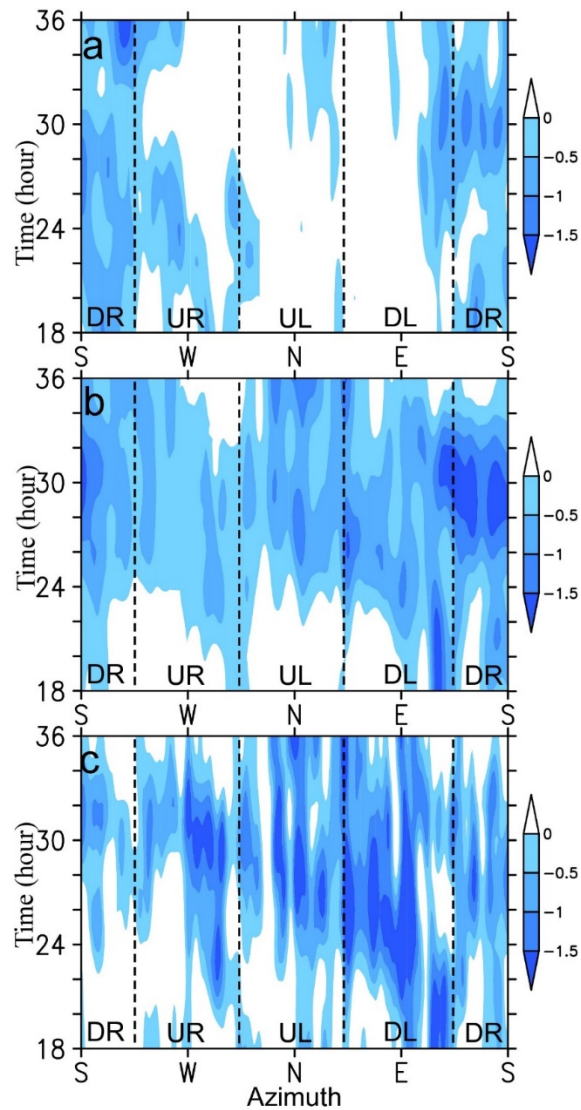


Figure. R3.7 Azimuthal-time cross-sections of the layer-mean (0.05-1.0 km) convergence (shaded, 10^{-4} s^{-1}) averaged from 80-km to 120-km radii of (a) NSEF,

(b) CTL, and (c) differences between CTL and NSEF. The black dashed lines indicate the quadrants relative to the large-scale vertical wind shear.

References:

- Wang, S., Montgomery, M.T. & Smith, R.K., 2021: Solutions of the Eliassen balance equation for inertially and/or symmetrically stable and unstable vortices. *Quarterly J. Royal Meteorol. Soc.*, 1–12. Available from: <https://doi.org/10.1002/qj.4098>.
- Heng, J., Wang, Y., and Zhou, W., 2017: Revisiting the balanced and unbalanced aspects of tropical cyclone intensification. *J. Atmos. Sci.*, 74, 2575–2591, <https://doi.org/10.1175/JAS-D-17-0046.1>.
- Montgomery, M.T. and Persing, J., 2021: Does balance dynamics well capture the secondary circulation and spin-up of a simulated tropical cyclone? *Journal of the Atmospheric Sciences*, 78, 75–95. Available from: <https://journals.ametsoc.org/view/journals/atsc/78/1/jas-d-19-0258.1.xml>.
- Wang S, Smith RK, Montgomery MT, 2020: Upper-tropospheric inflow layers in tropical cyclones. *Quarterly J. Royal Meteorol. Soc.*, 146, 3466–3487. Available from: <https://doi.org/10.1002/qj.3856>.